A PHYSICAL MODEL FOR PLANAR SPIRAL INDUCTORS ON SILICON

C. Patrick Yue, Changsup Ryu, Jack Lau*, Thomas H. Lee, and S. Simon Wong

Center for Integrated Systems, Stanford University, Stanford, CA 94305
*Dept. of Electrical and Electronic Eng., The Hong Kong University of Science & Technology

ABSTRACT

This paper presents a physical model for planar spiral inductors on silicon. The model has been confirmed with measured and published data of inductors having different geometric and process parameters. This model is scalable with inductor geometry, allowing designers to predict and optimize the quality factor.

INTRODUCTION

Interest in monolithic spiral inductors has surged with recent growing demand for Si-based RF communication circuits [1]. Although promising experimental results [2][3] have been reported, basic understanding of the performance limitations and procedures for optimizing the quality factor, Q, are lacking. A scalable physical model that can accurately predict the behavior of inductors with different structural parameters over a broad range of frequency would be a valuable RF IC design tool. Each element of the model should be consistent with the physical phenomena occurring in the part of the structure it represents. In particular, the physical model should account for eddy current effect in the spiral conductor, crossover capacitance between the spiral and the center-tap, capacitance between the spiral and the substrate, substrate ohmic loss, and substrate capacitance.

PHYSICAL INDUCTOR MODEL

A. Inductor Model Description

Fig. 1 shows the physical model of an inductor on silicon with one end and the substrate grounded. The series branch consists of L_s, R_s, and C_s. L_s represents the series inductance and is computed using the Greenhouse algorithm [4]. The series resistance, R_s, takes into account the skin depth of a conductor with finite thickness [5] and the current distribution in a microstrip conductor [6]. The series feed-forward capacitance, C_s, is approximated as the parallel-plate capacitance between the spiral and the center-tap underpass [7]. C_{ox} represents the capacitance between the spiral and the substrate. The silicon substrate is modeled by C_{si} and R_{si} [2][8][9]. C_{ox}, C_{si}, and R_{si} are proportional to the area covered by the spiral. C_{sub} and G_{sub} are the properties of the silicon substrate and are extracted from measured data.

$$R_s = \frac{\rho \cdot l}{w \cdot \delta \cdot (1 - e^{-t/\delta})}$$

$$C_s = n \cdot w^2 \cdot \frac{\varepsilon_{ox}}{t_{\text{ox M1-M2}}}$$

$$C_{ox} = \frac{1}{2} \cdot l \cdot w \cdot \frac{\varepsilon_{ox}}{t_{\text{ox}}}$$

$$C_{si} = \frac{1}{2} \cdot l \cdot w \cdot C_{Sub}$$

$$R_{si} = \frac{2}{l \cdot w \cdot G_{Sub}}$$

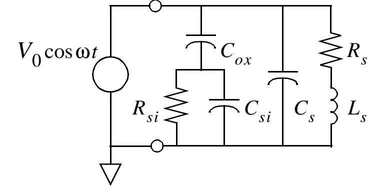

Fig. 1 Physical model of an inductor on silicon. (ρ = metal resistivity at dc, l = overall length of spiral, w = line width, δ = metal skin depth, t = metal thickness, N = number of turns, n = number of crossovers between spiral and center-tap = $N - 1$, $t_{ox\,M1\text{-}M2}$ = oxide thickness between spiral and center-tap, t_{ox} = oxide thickness between spiral and substrate, C_{sub} = substrate capacitance per unit area, G_{sub} = substrate conductance per unit area)

B. Definition of Quality Factor

The efficiency of an inductor is measured by its Q, which is limited by the parasitics. The energy storage and loss mechanisms in an inductor on silicon can be described by an equivalent energy model (Fig. 2), where L_s, R_s, R_p, and C_o represent the overall inductance, conductor loss, substrate loss, and overall capacitance respectively. Note that R_p and C_p represent the combined effects of C_{ox}, C_{si}, and R_{si}, and hence are frequency dependent. Combining the energy terms in Fig. 2 according to the fundamental definition of Q yields [10]

$$\begin{aligned} Q &= 2\pi \frac{|Peak\ Magnetic\ Energy - Peak\ Electric\ Energy|}{Energy\ Loss\ in\ One\ Oscillation\ Cycle} \\ &= \frac{\omega L_s}{R_s} \times \frac{R_p}{R_p + [(\omega L_s/R_s)^2 + 1] \cdot R_s} \times \left(1 - \frac{R_s^2 C_o}{L_s} - \omega^2 L_s C_o\right) \end{aligned} \quad (1)$$

where $\omega L_s/R_s$ accounts for the magnetic energy stored and the ohmic loss in the spiral conductor. The second term is the substrate loss factor representing the energy dissipated in the semiconducting silicon substrate. The last term is the self-resonance factor describing the reduction in Q due to the

$$E_{E\,Peak} = \frac{V_0^2 C_o}{2}$$

$$E_{M\,Peak} = \frac{V_0^2 L_s}{2 \cdot [(\omega L_s)^2 + R_s^2]}$$

$$E_{Loss} = \frac{2\pi}{\omega} \cdot \frac{V_0^2}{2} \cdot \left[\frac{1}{R_p} + \frac{R_s}{(\omega L_s)^2 + R_s^2}\right]$$

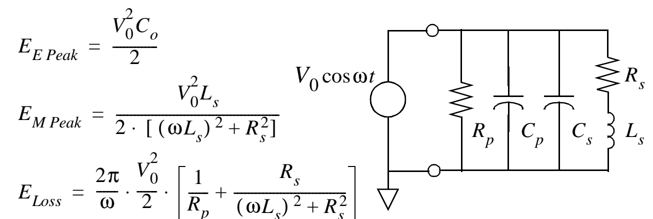

Fig. 2 Equivalent energy model representing the energy storage and loss mechanisms in a monolithic inductor. Note that $C_o = C_p + C_s$.

increase in the peak electric energy with frequency and the vanishing of Q at the self-resonant frequency.

C. Experiments and Parameter Extraction

Square spiral inductors with different structural and process parameters were fabricated with standard silicon processing technology and their two-port S parameters were measured using an HP8720B Network Analyzer and Cascade Microtech coplanar ground-signal-ground probes. During the measurements, the silicon substrate was grounded from the backside through the testing chuck. The parasitics of the probe pads were de-embedded using open dummy structures. Then, the lumped elements in the inductor model were extracted from the complex propagation constant and characteristic impedance [5] using the procedure outlined in Fig. 3.

D. Verification of the Physical Model

The measured and modeled values of the individual elements are plotted in Fig. 4 for two 8-nH inductors. L_s and R_s are subject to eddy current effect in the conductor. At high frequencies, the penetration of magnetic field into the conductor is attenuated, which causes reduction in the magnetic flux internal to the conductor [11]. However, L_s does not decrease significantly with increasing frequency because it is predominantly determined by the magnetic flux external to the conductor. Thus, it is valid to model L_s as a constant. The skin effect on R_s is more pronounced because R_s is inversely proportional to the effective cross-sectional area. C_s is independent of frequency since it represents the metal-to-metal cross-over capacitance between the spiral and the center-tap; its extracted and modeled values are 26 and 28 fF respectively. The frequency behaviors of R_p and C_p are governed by C_{ox}, C_{si}, and R_{si}. At low frequencies, the electric field terminates at the oxide-Si interface and C_p is primarily determined by C_{ox}. Since almost all energy is transmitted within the oxide layer along the spiral, little conduction current flows in the silicon substrate and thus R_p is large [5]. As frequency increases, the electric field starts to penetrate into the silicon substrate which reduces C_p because of the series connection of oxide and silicon substrate capacitances. The roll-off in R_p signifies increasing energy transmission and hence more dissipation in the silicon substrate. At high frequencies, energy is transmitted mainly within the silicon substrate causing C_p and R_p to approach C_{si} and R_{si} respectively; C_{ox} is effectively short-circuited. Fig. 5(a) illustrates that at low frequencies, Q is well described by $\omega L_s/R_s$. The rapid degradation of Q at high frequencies is a combined effect of the substrate loss and the self-resonance (Fig. 5(b)).

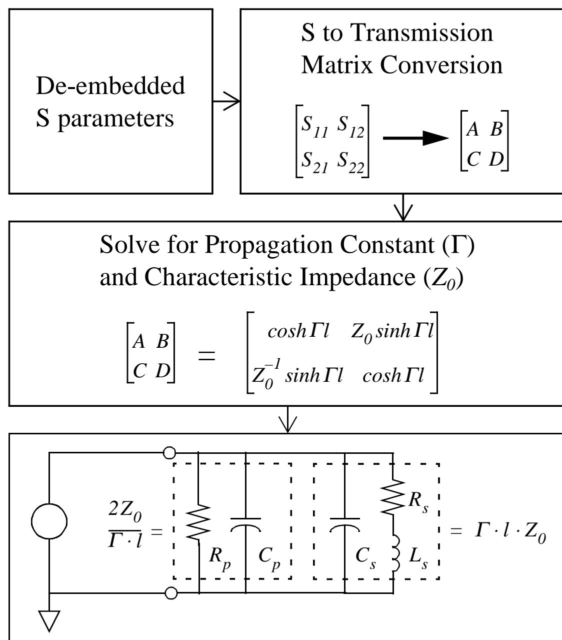

Fig. 3 Testing and parameter extraction procedure for the lumped elements in the inductor model.

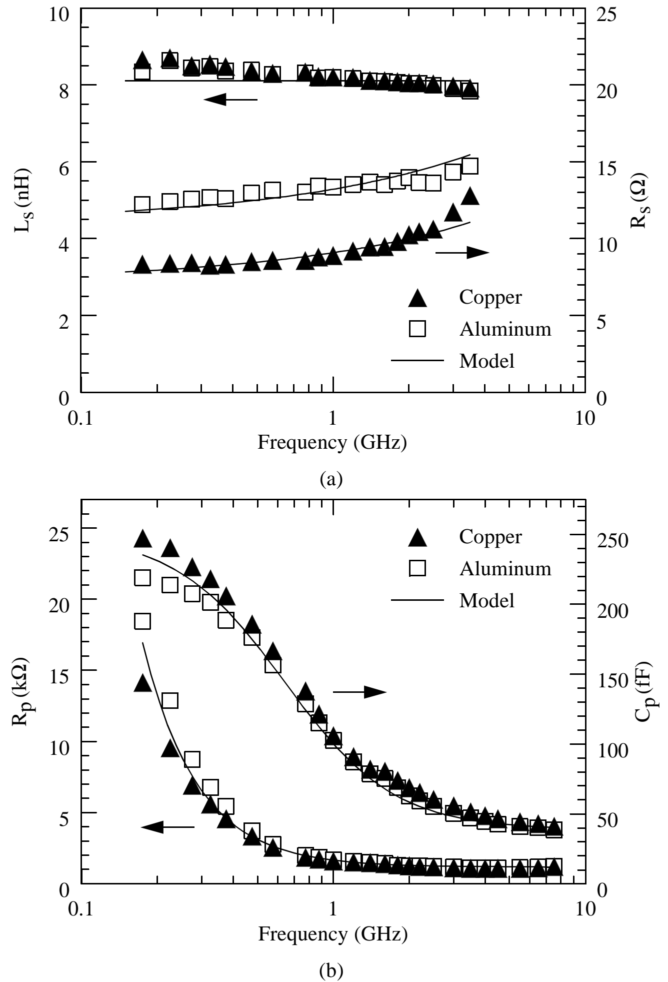

Fig. 4 The measured and modeled values of (a) L_s and R_s and (b) R_p and C_p for 1 µm thick spirals in copper (ρ_{Cu} = 2 µΩ-cm) and aluminum (ρ_{Al} = 3 µΩ-cm). (N = 7, w = 13 µm, l = 4.4 mm, t_{ox} = 4.5 µm, $t_{ox\,M1\text{-}M2}$ = 1.3 µm, C_{sub} = 1.6×10^{-3} fF/µm^2, G_{sub} = 4×10^{-8} S/µm^2, line spacing (s) = 7 µm, and outer dimension (OD) = 300 µm)

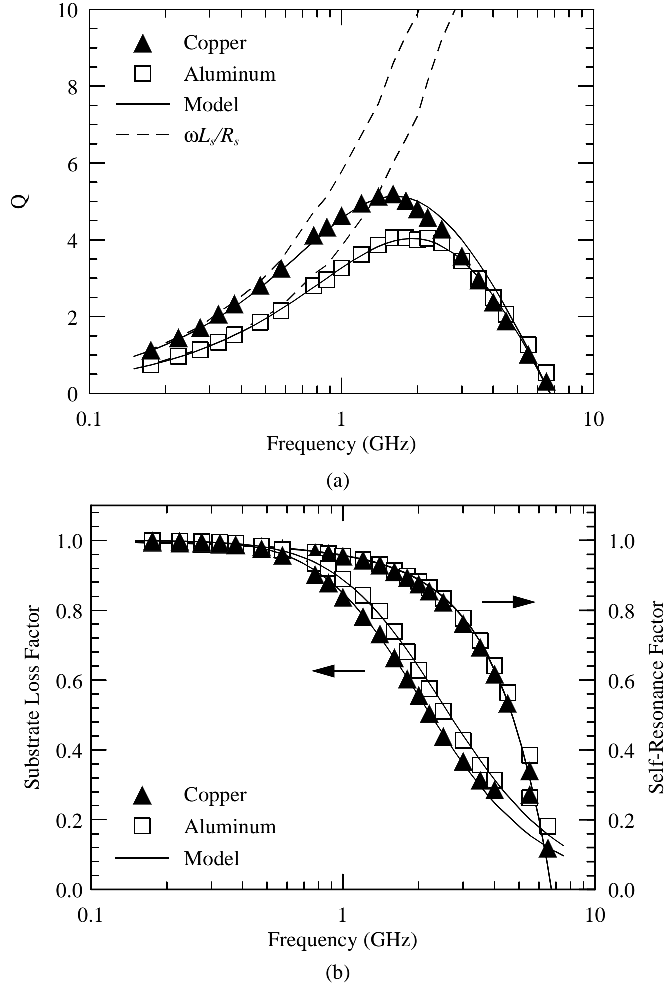

Fig. 5 The measured and modeled values of (a) Q and (b) substrate loss factor and self-resonance factor for the inductors in Fig. 4.

RESULTS AND DISCUSSION

To demonstrate the scalability of our model, we tested inductors with various structural parameters. Fig. 6 shows the effect of different metal schemes on Q. At 1 GHz, the effective thicknesses of 1 µm and 3 µm Al are 0.84 µm and 1.83 µm respectively using the formula in Fig. 1. After including the substrate factors, the ratio between their Q's at 1 GHz is two. The single-level 3-µm and triple-level 1-µm cases have the same Q since the former suffers from strong self-induced eddy current, and the latter from the combination of self and mutual eddy currents. Fig. 7 illustrates that increasing oxide thickness improves the Q since the substrate loss and self-resonance effects are suppressed. But as frequency increases, the effect of C_{ox} vanishes and the Q's merge together. Lowering the silicon substrate resistivity decreases R_{si} and increases C_{si}, causing the Q roll-off to occur at a lower frequency and a reduction of the self-resonant frequency (Fig. 8). Fig. 9 illustrates the effect of layout area on Q for the same inductance. The larger area inductors have higher Q's at low frequencies because of lower series resistance. As frequency increases, the substrate effects begin to dominate and the larger area inductors actually have lower Q's. Fig. 10 compares the measured Q_{peak} of the inductors presented by Ashby *et al.* [2] and the Q values predicted by

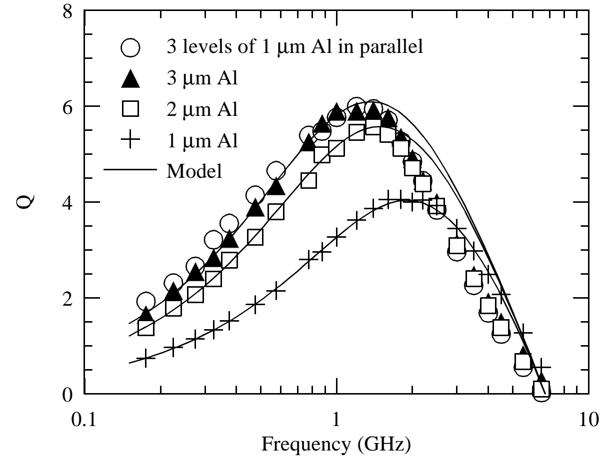

Fig. 6 The effect of metal scheme on Q. (L_s = 8 nH, t_{ox} = 4.5 µm, ρ_{si} = 10 Ω-cm, N = 7, w = 13 µm, s = 7 µm, OD = 300 µm)

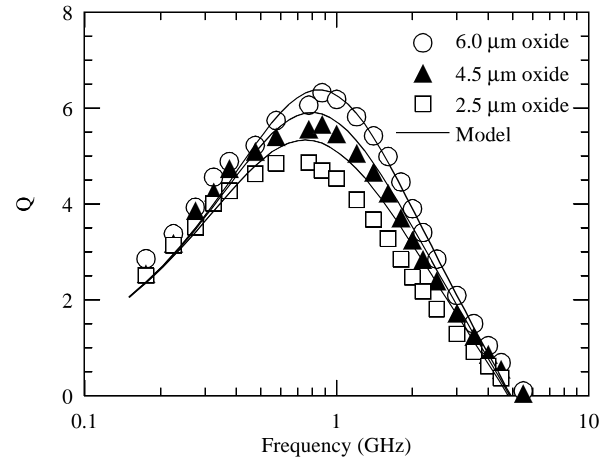

Fig. 7 The effect of oxide thickness on Q. (L_s = 8 nH, t_{Al} = 3 µm, ρ_{si} = 10 Ω-cm, N = 6, w = 24 µm, s = 7 µm, OD = 400 µm)

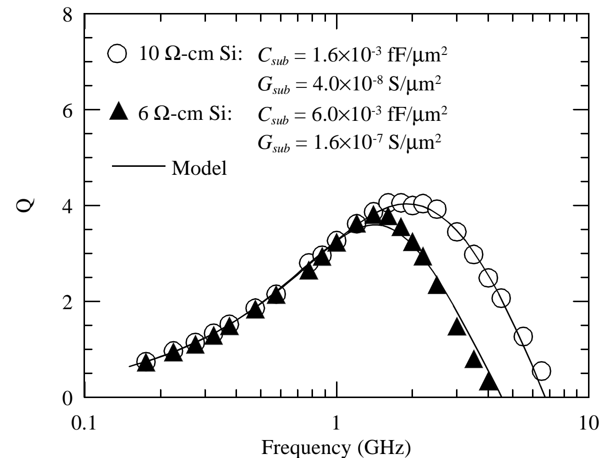

Fig. 8 The effect of substrate resistivity on Q. (L_s = 8 nH, t_{ox} = 4.5 µm, t_{Al} = 1 µm, N = 7, w = 13 µm, s = 7 µm, OD = 300 µm)

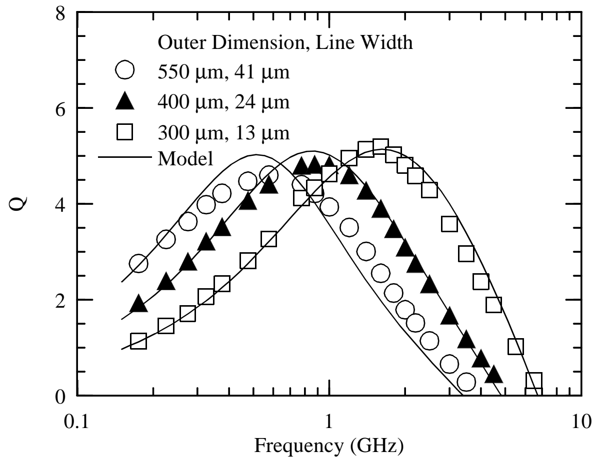

Fig. 9 The effect of layout area on Q. (L_s = 8 nH, t_{ox} = 4.5 µm, t_{Cu} = 1 µm, ρ_{si} = 10 Ω-cm, s = 7 µm)

our model. Excellent agreement is obtained.

In Fig. 11, we present Q contour plots generated using our model along with some experimental data. Q is plotted as a function of inductance and outer dimension of square spiral inductors. These contour plots serve as a design tool for achieving a specific inductance with the highest Q possible for a given technology at the frequency of interest.

CONCLUSIONS

A physical model for planar spiral inductors on silicon is presented. Physical phenomena important to the prediction of Q are considered and analyzed. The scalable inductor model shows good agreement with measured and published data.

ACKNOWLEDGMENTS

The authors would like to thank the Stanford CIS staff for their assistance in processing. This work has been supported by the CIS industrial sponsors and NSF contract MIP-9313701.

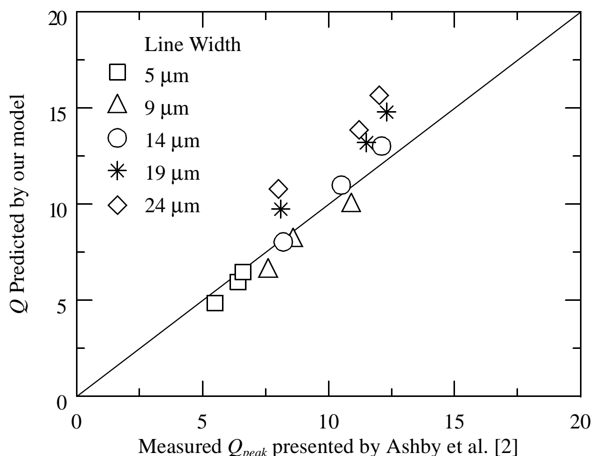

Fig. 10 Verification of the physical model using published data. (C_{sub} = 4.0×10^{-3} fF/µm^2, G_{sub} = 1.7×10^{-8} S/µm^2, s = 4 µm, OD = 300 µm)

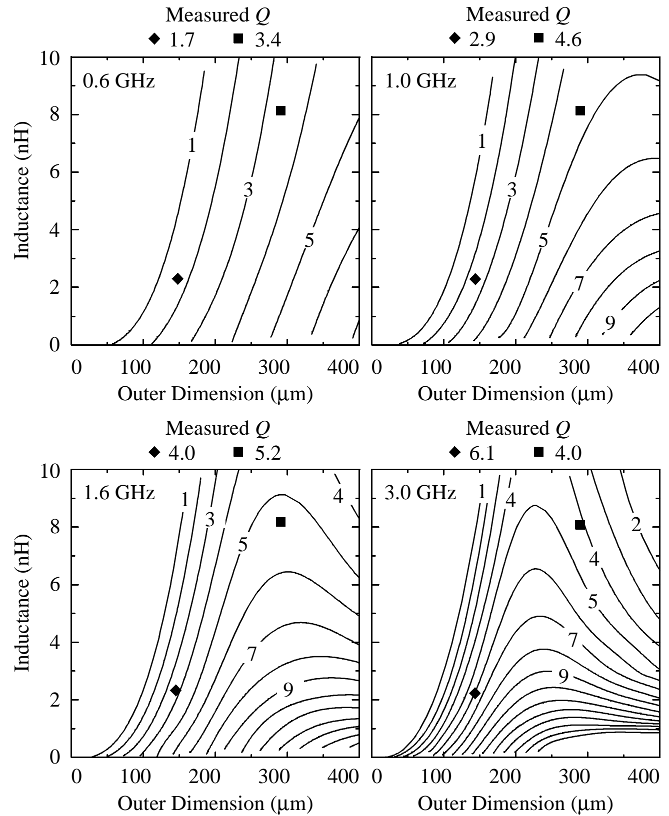

Fig. 11 Contour plots of Q as a function of inductance and outer dimension of square spiral inductors. (t_{ox} = 4.5 µm, t_{Cu} = 1 µm, ρ_{Cu} = 2 µΩ-cm, ρ_{si} = 10 Ω-cm, s = 7 µm)

REFERENCES

[1] P. R. Gray and R. G. Meyer, “Future directions in silicon ICs for RF personal communications,” *Proceedings of the IEEE 1995 Custom Integrated Circuits Conference*, pp. 83-90, May 1995.

[2] K. B. Ashby, I. A. Koullias, W. C. Finley, J. J. Bastek, and S. Moinian, "High Q inductors for wireless applications in a complementary silicon bipolar process," *IEEE JSSC*, vol. 31, no. 1, pp. 4-9, Jan. 1996.

[3] J. N. Burghartz, M. Soyuer, and K. A. Jenkins, "Microwave inductors and capacitors in standard multilevel interconnect silicon technology," *IEEE Trans. MTT*, vol. 44, no. 1, pp. 100-104, Jan. 1996.

[4] H. Greenhouse, "Design of planar rectangular microelectronic inductors," *IEEE Trans. PHP*, vol. 10, no.2, pp. 101-109, June 1974.

[5] Y. Eo and W. R. Eisenstadt, "High speed VLSI interconnect modeling based on S-parameter measurements," *SRC Pub C93337*, July 1993.

[6] R. A. Pucel, D. J. Massé, and C. P. Hartwig, “Losses in microstrip,” *IEEE Trans. MTT*, vol. 16, no.6, pp. 342-350, Jun. 1968.

[7] L. Wiemer and R. H. Jansen, “Determination of coupling capacitance of underpasses, air bridges and crossings in MICs and MMICs,” *Electronics Letters*, vol. 23, no. 7, pp. 344-346, Mar. 1987.

[8] I. T. Ho and S. K. Mullick, “Analysis of transmission lines on integrated-circuit chips,” *IEEE JSSC*, vol. 2, no. 4, pp. 201-208, Dec. 1967.

[9] H. Hasegawa, M. Furukawa, and H. Yanai, "Properties of microstrip line on Si-SiO_2 system," *IEEE Trans. MTT*, vol. 19, no. 11, pp. 869-881, Nov. 1971.

[10] H. G. Booker, Energy in Electromagnetism, London, New York: Peter Peregrinus on behalf of the Institution of Electrical Engineers, 1982.

[11] H. A. Wheeler, “Formulas for the skin effect,” *Proceedings of I.R.E.*, vol. 30, pp. 412-424, Sept. 1942.